

## EFFECTS OF FRONTAL AND PLAN SOLIDITY ON ROUGH-WALL TURBULENT CHANNEL FLOW OVER PYRAMID ROUGHNESS

**Oleksandr Zhdanov**

James Watt School of Engineering  
University of Glasgow  
Glasgow, United Kingdom, G12 8QQ  
oleksandr.zhdanov@glasgow.ac.uk

**Angela Busse**

James Watt School of Engineering  
University of Glasgow  
Glasgow, United Kingdom, G12 8QQ  
angela.busse@glasgow.ac.uk

### ABSTRACT

Direct numerical simulations of turbulent flow over rough surfaces comprised of pyramids are conducted in a closed channel configuration at  $Re_\tau = 395$ . The effects of frontal and plan solidity on the fluid dynamic roughness effect in the ‘waviness’ regime are investigated. The frontal and plan solidity are systematically varied from 0.05 to 0.1 and from 0.25 to 1, respectively. The results show that both parameters have significant effect on the roughness function and mean flow and turbulence statistics. Frontal solidity influences the roughness function at any value of plan solidity, while plan solidity has a strong impact only at low frontal solidity. In addition, surfaces with peak-to-peak spanwise spacing comparable to the outer scale of the flow are found to generate secondary currents.

### INTRODUCTION

Prediction of the drag of rough surfaces based on their topography is a key challenge in fluid mechanics due to the wide range of roughness topographies found in engineering and geophysical applications (Jiménez, 2004; Flack & Schultz, 2010). Despite a significant body of work in this field, existing empirical formulae cover only a limited range of roughness topographies and further systematic studies are required (Chung *et al.*, 2021).

The effect of a rough surface on the mean flow is commonly expressed in terms of the Hama roughness function  $\Delta U^+$  (Hama, 1954), which represents the downward shift of the mean inner-scaled velocity profile in the log region compared to the smooth-wall case. Since the pioneering work of Schlichting (1937), rough surfaces composed of regular roughness elements are typically characterised by two density parameters, namely the frontal and the plan solidity. The frontal solidity ( $\lambda_f$ ) is the ratio of the total projected frontal area of the roughness elements to the total plan area. In turn, the plan solidity ( $\lambda_p$ ) is the fraction of the total plan area covered by roughness elements.



















Most previous experimental and numerical investigations on the effects of  $\lambda_f$  and  $\lambda_p$  have been conducted for surfaces with regular arrangements of cubical roughness elements (see,

e.g., Cheng *et al.*, 2007; Leonardi & Castro, 2010). While these investigations provide valuable insights, their main limitation is the fact that by definition of a cube  $\lambda_f = \lambda_p$ ; thus, it is impossible to explore the relative effects of these two parameters. Placidi & Ganapathisubramani (2015, 2018) used a different approach and separated the effects of frontal and plan solidity by combining LEGO<sup>®</sup> bricks in different configurations keeping one of the parameters (either  $\lambda_f$  or  $\lambda_p$ ) constant while varying the other. In contrast to studies with cubical roughness in standard configurations, they found a peak in the roughness effect only for variations in  $\lambda_f$  at constant  $\lambda_p$ , while at constant  $\lambda_f$  drag monotonically decreased with an increase in  $\lambda_p$ , showing that these two parameters can influence rough-wall behaviour in differing ways.

Another feature of surfaces comprised of cubical roughness elements is the fact that in the extreme case of plan solidity approaching unity ( $\lambda_p \rightarrow 1$ ), the rough surface merges into a smooth wall elevated by the roughness height. However, using other 3D roughness elements, e.g., pyramids, it is possible to create fully covered surfaces that remain rough. Schultz & Flack (2009) experimentally studied rough surfaces comprised of close-packed pyramids ( $\lambda_p = 1$ ) while systematically varying their frontal solidity. Their results show that at low  $\lambda_f$  the roughness function does not scale with roughness height and term surface ‘waviness’ was proposed to describe the behaviour of these surfaces. However, the effects of plan solidity have not been considered and it is not clear whether these observations will hold for  $\lambda_p < 1$ . In this context it is also interesting to note that Nugroho *et al.* (2021) showed that for irregular surfaces with low effective slope ( $ES = 2\lambda_f$ ) non k-type behaviour is observed when the in-plane roughness wavelength is comparable to the boundary layer thickness.

In the present study the effects of plan and frontal solidity are studied numerically for surfaces covered with pyramid-shaped roughness elements in different configurations. The aim of this investigation is to explore individual effects of  $\lambda_f$  and  $\lambda_p$  on the fluid dynamic roughness effect. The focus of the current study is the low effective slope or ‘sparse’ regime, i.e., surfaces that would fall under the ‘waviness’ regime following the classification of Schultz & Flack (2009).

Table 1. Key topographical parameters of the investigated surfaces:  $\lambda_f$  - frontal solidity,  $\lambda_p$  - plan solidity,  $S_z$  - maximum peak to valley height,  $z_0$  - smooth-wall displacement, which is equal to the roughness mean height  $\langle h(x,y) \rangle$  in the present study,  $W$  - spanwise peak-to-peak distance.

Case	1	2	3	4	5	6	7	8	9
$\lambda_f$	0.05	0.075	0.1	0.05	0.075	0.1	0.05	0.075	0.1
$\lambda_p$	1	1	1	0.444	0.444	0.444	0.25	0.25	0.25
$S_z/\delta$	0.1	0.1	0.1	0.1	0.1	0.1	0.1	0.1	0.1
$-z_0/\delta$	0.033	0.033	0.033	0.0148	0.0148	0.0148	0.00833	0.00833	0.00833
$W/\delta$	1	0.667	0.5	0.667	0.444	0.333	0.5	0.333	0.25
Line style									
Marker									

## METHODOLOGY

Nine different surfaces were constructed using pyramid-shaped roughness elements. The pyramids are similar to those used by Schultz & Flack (2009), i.e., they have a square base with an edge facing the flow and a staggered arrangement is employed. In all cases, the roughness elements have a fixed height of  $0.1\delta$ , where  $\delta$  is the mean channel half-height.

The number and slope of the pyramids are systematically varied to change either the frontal solidity at constant plan solidity or vice versa. The topographical parameters for the surfaces are summarised in Table 1. The plan solidity,  $\lambda_p$ , is varied from 1 (closely packed) to 0.25 by moving the pyramids further apart (see Figure 1). For fixed plan solidity, the frontal solidity,  $\lambda_f$ , is varied by changing the height-to-base ratio of the pyramids, i.e., by modifying the inclination angle of the pyramids' edges. All values of the frontal solidity fall into the low frontal solidity regime ( $\lambda_f \leq 0.1$ ), where a reduction in the roughness effect is expected with decreasing  $\lambda_f$  (Jiménez, 2004). Based on their effective slope values, all nine cases should fall under the 'waviness' regime. The peak-to-peak spacing of the pyramids,  $W$ , decreases with decreasing  $\lambda_p$  and increasing  $\lambda_f$ . The roughness mean height,  $\langle h(x,y) \rangle$ , which in the present study is equal to the smooth-wall offset,  $z_0$ , applied in each simulation, is only influenced by the plan solidity  $\lambda_p$  but independent of  $\lambda_f$  due to the fixed maximum peak-to-valley height,  $S_z$ , which corresponds for the present surfaces to the pyramid height.

For each configuration a direct numerical simulation of a fully developed turbulent channel flow at friction Reynolds number  $Re_\tau = u_\tau \delta / \nu = 395$  is conducted to obtain the fluid dynamic properties of the surface using the DNS code iIMB (Busse *et al.*, 2015). Flow statistics are acquired in each case for over 100 flow through times after a statistically stationary flow has been attained. To compute statistical quantities the double-averaging approach of Raupach & Shaw (1982) is used. The rough surfaces are resolved using an iterative version of the embedded boundary method of Yang & Balaras (2006). The pyramid roughness is applied to both the lower and the upper wall of the channel. To minimise any local blockage effects, the roughness on the upper wall is shifted by half of the minimum repeating unit length in the streamwise direction. An offset  $z_0$ , is applied so that the  $z = 0$  location corresponds to the roughness mean plane, setting the mean channel height to  $2\delta$  in all conducted simulations.

For all cases except case 5, the domain size in stream-

wise and spanwise directions is set to  $8\delta \times 4\delta$ . For case 5 a slightly lower domain size ( $7.11\delta \times 3.55\delta$ ) is used to maintain an integer number of pyramids. The grid spacing is uniform in the streamwise and spanwise directions with  $\Delta x^+ = \Delta y^+ < 5$  and is adjusted to maintain at least 36 grid points per pyramid in each direction. The wall-normal grid spacing is constant across the roughness height  $\Delta z_{min}^+ = 2/3$  and is gradually increased above, reaching its maximum value  $\Delta z_{max}^+ < 5$  at the channel centre.

## RESULTS AND DISCUSSION

### Mean velocity profiles

Mean streamwise velocity profiles for all considered cases are presented in Figure 2a together with smooth-wall reference data at the same friction Reynolds number. With the increase of  $\lambda_f$  at constant plan solidity the downward shift in the mean streamwise velocity profile increases, indicating an enhancement of the roughness effect. With a decrease of  $\lambda_p$  at fixed frontal solidity, the observed effect is similar. However, the mean velocity profiles for the two lowest values of  $\lambda_p$  at the two highest values of  $\lambda_f$  are very close to each other (cases 5 & 8 and 6 & 9), suggesting that the effect of plan solidity on the mean velocity profile saturates for low values of  $\lambda_p$ .

Streamwise velocity profiles in the defect form are plotted in Figure 2b. A good collapse between smooth- and rough-wall data is observed at wall-normal locations  $z/\delta > 0.5$ . Closer to the roughness crest, the profile shapes differ between most cases, which can be attributed to the presence of large secondary currents in cases 1, 2, and 4 or a shift of the virtual origin of the studied surfaces. This is in line with observations by Chan *et al.* (2018) for egg-carton surfaces with decreasing wavelength.

### Roughness function

The roughness function for all considered surfaces is plotted against the effective slope, which is directly related to frontal solidity ( $ES = 2\lambda_f$ ), in Figure 3a and against plan solidity in Figure 3b. In addition, data by Napoli *et al.* (2008), Schultz & Flack (2009), and Chan *et al.* (2018) is also included.

The  $\Delta U^+$  values were determined based on the difference in centreline velocity of the rough and smooth wall profiles. An alternative method for measuring  $\Delta U^+$  was also tested: the roughness function was evaluated at the height of 50 wall units

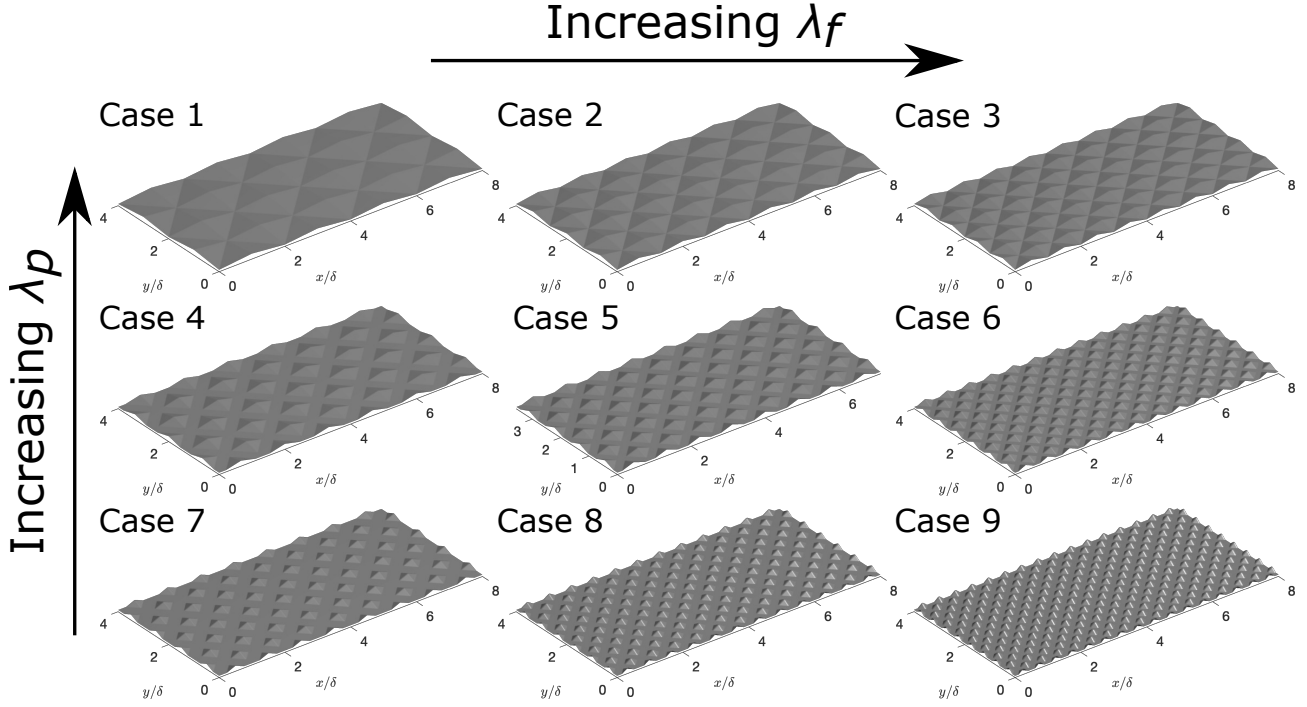


Figure 1. Illustration of the studied surfaces composed of pyramid-shaped roughness elements. Surfaces with varying frontal solidity at constant plan solidity are presented in horizontal rows. Surfaces with varying plan solidity at constant frontal solidity are presented in vertical columns.

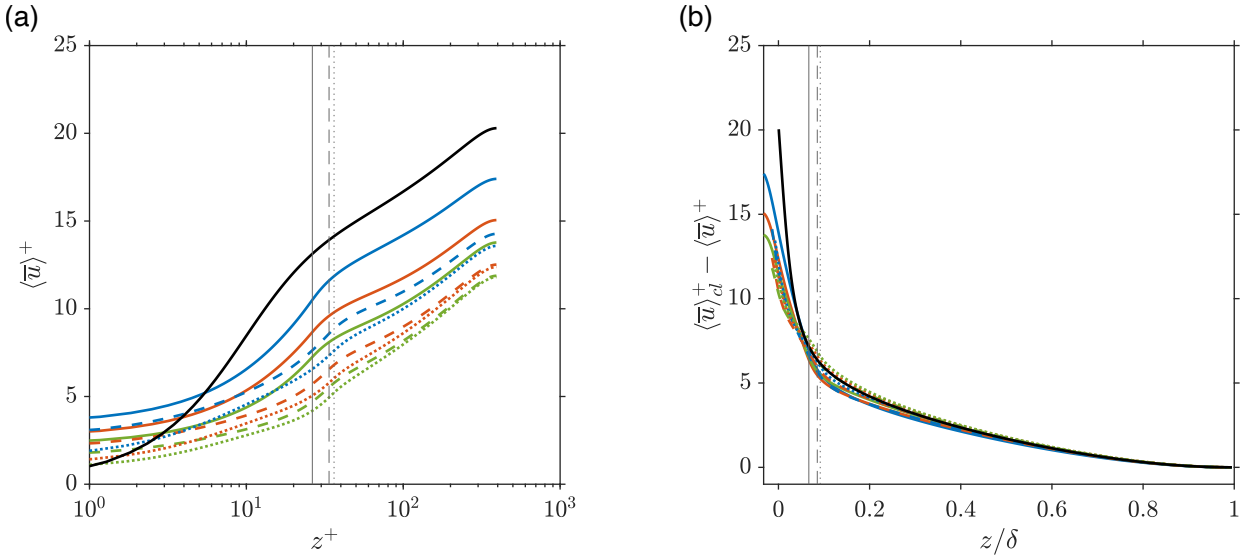


Figure 2. (a) Mean streamwise velocity profiles; (b) Streamwise velocity defect profiles for all studied surfaces. Line styles and colours are specified in Table 1. Reference smooth-wall data is also shown with a solid black line. The location of the maximum roughness height for each surface is indicated by a thin vertical line with a corresponding line style.

above the roughness crest, as in Chan *et al.* (2015) for egg-carton roughness in the transitionally rough regime, to check the influence of the applied approach to determine  $\Delta U^+$ . The difference in  $\Delta U^+$  determined by both methods is below 10% for all cases except for case 1, where the difference is 17%. The higher difference for case 1 can be attributed to the presence of strong secondary flows. However, this does not affect the observed trends in  $\Delta U^+$  with variation of frontal and plan solidity.

Both  $\lambda_f$  and  $\lambda_p$  have a clear effect on the roughness function but, as can be seen from Figure 3, these parameters influence  $\Delta U^+$  in opposite ways. Frontal solidity influences the

values of roughness function at any plan solidity. Increase in  $\lambda_f$  at constant plan solidity results in higher drag (Figure 3a). A more complex picture emerges for the dependency of  $\Delta U^+$  on plan solidity: while for high plan solidities range an increase in the roughness function with a decrease in  $\lambda_p$  is observed (see Figure 3b), the influence of plan solidity starts to saturate for surfaces with  $\lambda_p \leq 0.444$ . The effect of plan solidity is more pronounced at low values of frontal solidity. Cases with  $\lambda_p = 1$  and / or  $\lambda_f = 0.05$  generate significant secondary currents. This can be attributed to the fact that these cases have a high spanwise peak-to-peak distance between pyramids.

Comparing to the published data for other rough surfaces,

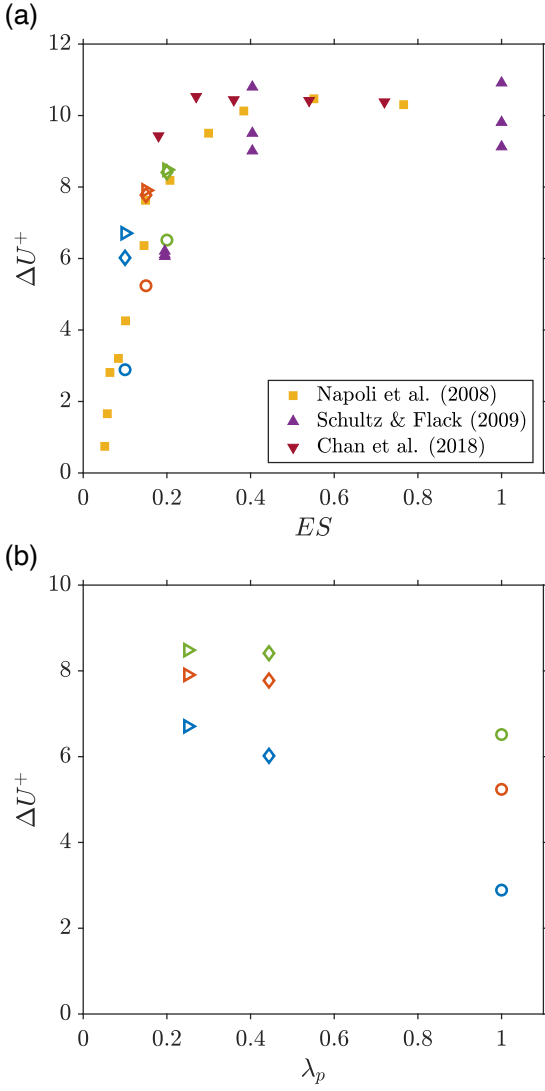


Figure 3. Roughness function as a function of (a) effective slope ( $ES = 2\lambda_f$ ) and (b) plan solidity. The data from literature for different rough surfaces is included for comparison. Present data markers are specified in Table 1.

the same increasing trend of  $\Delta U^+$  with effective slope / frontal solidity is observed in all cases. A good match between present results and the irregular 2D roughness by Napoli *et al.* (2008) is observed at  $ES \geq 0.15$ . However, a significant scatter in the values of roughness function between present data and the simulations of Napoli *et al.* (2008) is observed at low values of  $ES$ , which can be attributed to the effect of plan solidity. In addition, the value of the roughness function for case 3 ( $ES = 0.2$ ,  $\lambda_p = 1$ ) is close to those reported by Schultz & Flack (2009) for the same type of roughness as considered in this study with similar  $ES$ , but at much higher  $Re_\tau$ .

### Turbulence statistics

Double-averaged profiles of streamwise, wall-normal, and shear Reynolds and dispersive stresses are presented in Figure 4. To facilitate observations of the peak behaviour with variation of frontal and plan solidity, in the insets to parts of Figure 4 the profiles for each surface are shifted by their smooth-wall displacement,  $z_0$ , so that the location of the roughness crest coincides for all cases. The double-averaged streamwise normal Reynolds stress profiles demon-

strate a good collapse in the outer layer for all cases (Figure 4a). Compared to the smooth-wall case, a reduction of  $\langle u'u' \rangle^+$  is observed in the near wall region. With the increase in frontal solidity at constant  $\lambda_p$  the peak value of the streamwise turbulent fluctuations drops. The same effect is found when plan solidity is reduced while  $\lambda_f$  is kept constant. This is consistent with the observed increase of the roughness function and the results of Leonardi & Castro (2010) for cube roughness, where with increase of roughness solidity a reduction of the peak value of the streamwise Reynolds stress was reported. The peaks are located above the roughness crest, except for case 1, where the peak falls within roughness canopy.

The wall-normal Reynolds stresses are much less affected by the variation in frontal and plan solidity (Figure 4c). Their profiles also demonstrate a reasonable collapse in the outer layer for all cases. For rough surfaces comprised of staggered cubes, Leonardi & Castro (2010) found that the peak value of the wall-normal Reynolds stress decreases with the increase in roughness density. However, this behaviour is not consistently observed for the surfaces considered in the present study. With the increase in  $\lambda_f$  at constant plan solidity the peak value of wall-normal turbulent fluctuations slightly decreases. However, surfaces where high levels of dispersive stresses and consequently strong secondary currents are observed (cases 1, 2, and 4), do not follow this trend and their peak values are reduced compared to the surfaces with the same  $\lambda_p$  but without strong secondary currents. As a result, the trend is reversed for cases 1, 2, and 3, where surfaces with higher frontal solidity have higher peak values of  $\langle w'w' \rangle^+$ .

Reynolds shear stress profiles are plotted in Figure 4e. In all cases Reynolds shear stress levels are reduced compared to the smooth-wall case and show a good collapse in the outer layer. The most notable outlier is case 1, where a reduction of the Reynolds shear stress is observed up to wall-normal location  $z/\delta \approx 0.63$ . Overall, the wall-normal location where the  $-\langle u'w' \rangle^+$  profile of the rough surface collapses onto the smooth-wall data depends on the pyramids' peak-to-peak distance in spanwise direction. Surfaces with different solidities but equal  $W/\delta$  (see Table 1) collapse at approximately the same  $z/\delta$  onto the smooth-wall case, e.g., cases 2 and 4. With the decrease in  $W/\delta$  the location where the rough-wall profile collapses onto the smooth-wall data moves closer to the roughness crest. For surfaces with constant plan solidity, the peak value of the Reynolds shear stress rises with increase in  $\lambda_f$ , while for surfaces with constant frontal solidity peak values are reduced when  $\lambda_p$  is increased. However, case 1 does not follow these trends and its peak value of  $\langle u'w' \rangle^+$  is of similar magnitude as for the surfaces with the same plan solidity but higher  $\lambda_f$ .

For all studied surfaces the peak value of  $-\langle u'w' \rangle^+$  is observed above the maximum roughness height. The distance from the roughness crest to the peak location increases with a reduction in  $\lambda_f$  at constant plan solidity, and with an increase in  $\lambda_p$  at constant frontal solidity. Case 1 is an outlier from these trends again, and its peak location is closer to the roughness crest compared to the cases with the same  $\lambda_f$  or  $\lambda_p$ . In case 1 two peaks are observed, but due to similar values of  $-\langle u'w' \rangle^+$  at these peaks, the Reynolds shear stress profile appears almost constant above the maximum roughness height.

Profiles of dispersive stresses for all surfaces are shown in Figures 4b, d, and f. For cases 1, 2, 3, 4, and 7, where the spanwise peak-to-peak distance between pyramids is comparable to the channel half-height, elevated levels of all dispersive stresses can be observed well above roughness crest, indicating the presence of secondary currents. This is consistent with re-

sults for other rough surfaces, where secondary currents were reported when the spanwise spacing of the roughness elements (e.g., Zampiron *et al.*, 2020) or the roughness wavelength (e.g., Chan *et al.*, 2018) were similar to the outer scale of the flow. For case 1, which has the highest value of  $W/\delta$ , significant values of  $\langle \tilde{w}\tilde{w} \rangle^+$  and  $-\langle \tilde{u}\tilde{w} \rangle^+$  are observed up to  $z/\delta \approx 0.7$ , while  $\langle \tilde{u}\tilde{u} \rangle^+$  is elevated up to  $z/\delta \approx 0.5$ . The extent of all dispersive stresses in the wall-normal direction is dependent on  $W/\delta$  and decreases as  $W$  is reduced.

The peak value of streamwise dispersive stress is located below the roughness crest in all cases. In general, the peak values follow the same behaviour as the streamwise Reynolds stress, i.e., with an increase in frontal solidity at constant  $\lambda_p$  the peak value drops. Once again, case 1 does not follow this trend and its peak value is lower than for case 2, which has higher  $\lambda_f$ .

While for most cases peaks of  $\langle \tilde{w}\tilde{w} \rangle^+$  fall within the roughness canopy, the peak value for case 1 is located at the roughness crest (Figure 4d). No consistent behaviour is found for the wall-normal dispersive stress peak values with variation of  $\lambda_f$  or  $\lambda_p$ . While for surfaces with  $\lambda_p = 0.25$  the maximum value of  $\langle \tilde{w}\tilde{w} \rangle^+$  drops with an increase of  $\lambda_f$ , for cases 1, 2, and 3, where  $\lambda_p = 1$ , the peak value of  $\langle \tilde{w}\tilde{w} \rangle^+$  increases with frontal solidity.

For all cases with secondary currents, the  $-\langle \tilde{u}\tilde{w} \rangle^+$  profiles exhibit high levels above the roughness crest, with a second peak emerging in some cases. Case 1 again shows distinctive behaviour as the only case where a minimum and negative values for  $-\langle \tilde{u}\tilde{w} \rangle^+$  can be observed within the roughness canopy.

## CONCLUSIONS

Frontal and plan solidity of pyramid roughness has a significant effect on mean flow and turbulence statistics of rough-wall channel flow. The present study focuses on the ‘waviness’ regime, i.e., low effective slope cases. The roughness effect of the surface increases with frontal solidity at constant plan solidity, and decreases with increasing plan solidity at constant frontal solidity. Frontal solidity has a strong influence on  $\Delta U^+$  at any considered value of plan solidity, while a significant effect of  $\lambda_p$  is found at low  $\lambda_f$ , and the effect of plan solidity saturates once low plan solidity values are attained. Another significant parameter is the spanwise peak-to-peak distance between pyramids, which affects the extent of the dispersive stresses and formation of secondary currents. Dispersive stresses extend furthest into the flow for a spanwise peak-to-peak distance of the order of the channel half-height and their extent decreases with increase in frontal solidity due to reduction in the distance between adjacent peaks.

In the next stage of this project, an in-depth investigation of the secondary currents will be conducted and the structure of the turbulent flow will be investigated. In addition, simulations at different  $Re_\tau$  are planned to test for the Reynolds number dependency of the results.

## ACKNOWLEDGEMENTS

We gratefully acknowledge support by the United Kingdom’s Engineering and Physical Sciences Research Council under grant number EP/V002066/1.

## REFERENCES

Busse, A., Lützner, M. & Sandham, N. D. 2015 Direct numerical simulation of turbulent flow over a rough surface based on a surface scan. *Computers & Fluids* **116**, 129–147.

- Chan, L., MacDonald, M., Chung, D., Hutchins, N & Ooi, A. 2015 A systematic investigation of roughness height and wavelength in turbulent pipe flow in the transitionally rough regime. *Journal of Fluid Mechanics* **771**, 743–777.
- Chan, L., MacDonald, M., Chung, D., Hutchins, N & Ooi, A. 2018 Secondary motion in turbulent pipe flow with three-dimensional roughness. *Journal of Fluid Mechanics* **854**, 5–33.
- Cheng, H., Hayden, P., Robins, A. G. & Castro, I. P. 2007 Flow over cube arrays of different packing densities. *Journal of Wind Engineering and Industrial Aerodynamics* **95** (8), 715–740.
- Chung, D., Hutchins, N., Schultz, M. P. & Flack, K. A. 2021 Predicting the drag of rough surfaces. *Annual Review of Fluid Mechanics* **53**, 439–471.
- Flack, K. A. & Schultz, M. P. 2010 Review of hydraulic roughness scales in the fully rough regime. *Journal of Fluids Engineering* **132** (4), 041203.
- Hama, F. R. 1954 Boundary layer characteristics for smooth and rough surfaces. *Transactions of the Society of Naval Architects and Marine Engineers* **62**, 333–358.
- Jiménez, J. 2004 Turbulent flows over rough walls. *Annual Review of Fluid Mechanics* **36**, 173–196.
- Leonardi, S. & Castro, I. P. 2010 Channel flow over large cube roughness: a direct numerical simulation study. *Journal of Fluid Mechanics* **651**, 519–539.
- Napoli, E., Armenio, Vincenzo & De Marchis, M. 2008 The effect of the slope of irregularly distributed roughness elements on turbulent wall-bounded flows. *Journal of Fluid Mechanics* **613**, 385–394.
- Nugroho, B., Monty, J. P., Utama, I. K. A. P., Ganapathisubramani, B. & Hutchins, N. 2021 Non- $k$ -type behaviour of roughness when in-plane wavelength approaches the boundary layer thickness. *Journal of Fluid Mechanics* **911**, A1.
- Placidi, M. & Ganapathisubramani, B. 2015 Effects of frontal and plan solidities on aerodynamic parameters and the roughness sublayer in turbulent boundary layers. *Journal of Fluid Mechanics* **782**, 541–566.
- Placidi, M. & Ganapathisubramani, B. 2018 Turbulent flow over large roughness elements: effect of frontal and plan solidity on turbulence statistics and structure. *Boundary-layer Meteorology* **167** (1), 99–121.
- Raupach, Michael R & Shaw, RH 1982 Averaging procedures for flow within vegetation canopies. *Boundary-layer Meteorology* **22** (1), 79–90.
- Schlichting, H. 1937 Experimental investigation of the problem of surface roughness. *NACA Technical Memorandum* **823**.
- Schultz, M. P. & Flack, K. A. 2009 Turbulent boundary layers on a systematically varied rough wall. *Physics of Fluids* **21** (1), 015104.
- Yang, J. & Balaras, E. 2006 An embedded-boundary formulation for large-eddy simulation of turbulent flows interacting with moving boundaries. *Journal of Computational Physics* **215** (1), 12–40.
- Zampiron, A., Cameron, S. & Nikora, V. 2020 Secondary currents and very-large-scale motions in open-channel flow over streamwise ridges. *Journal of Fluid Mechanics* **887**, A17.

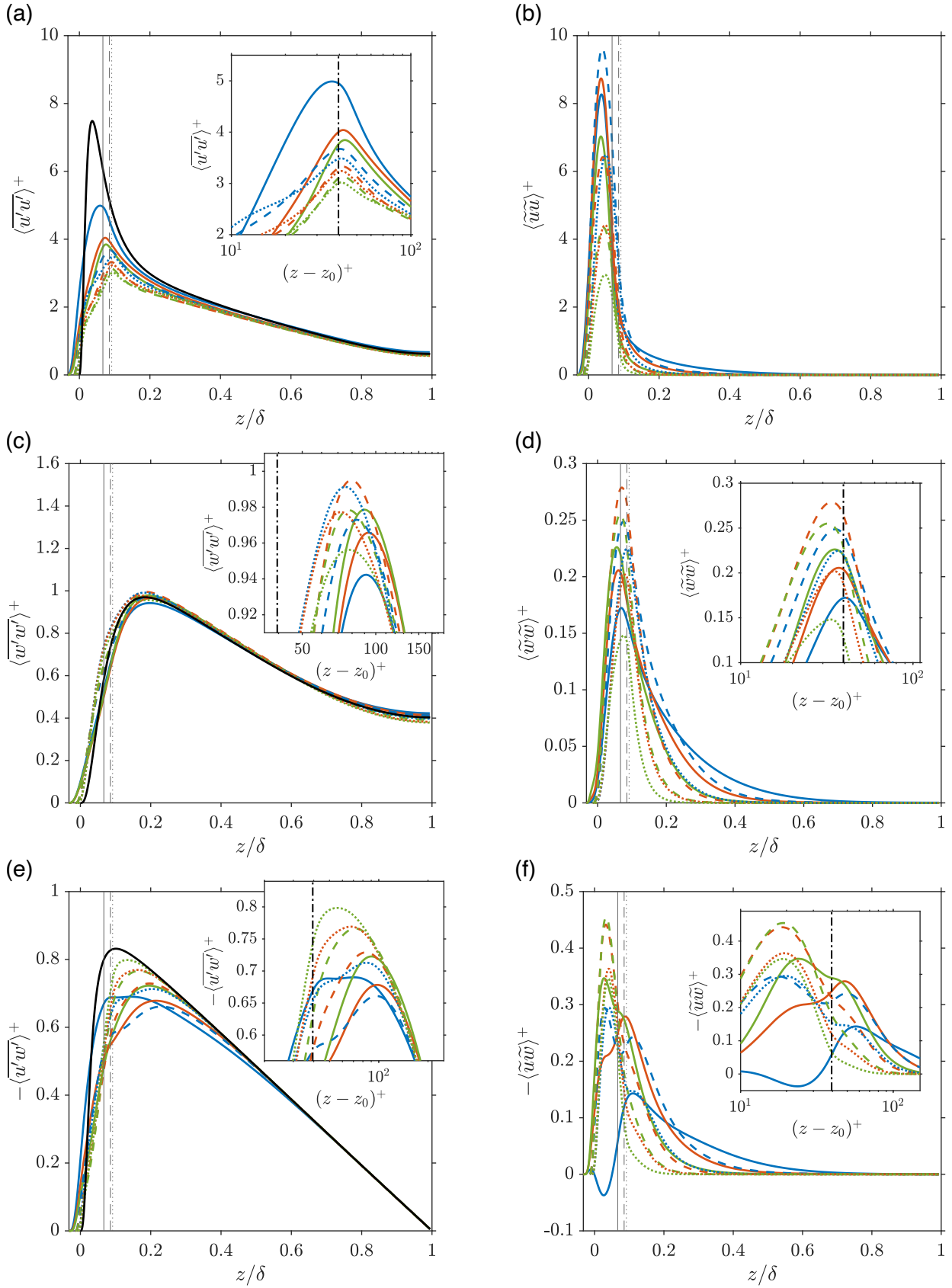


Figure 4. Double-averaged profiles of (a) Streamwise Reynolds normal stress; (b) Streamwise dispersive normal stress; (c) Wall-normal Reynolds normal stress; (d) Wall-normal dispersive normal stress; (e) Reynolds shear stress; (f) Dispersive shear stress for all studied surfaces. Line styles and colours are specified in Table 1. Reference smooth-wall data is also shown with a solid black line. The location of the maximum roughness height for each surface is indicated by a thin vertical line with a corresponding line style. An intrinsic averaging is employed in all cases.